A $^3\Pi_u$ ← X $^3\Sigma_g^-$ Electronic Spectrum of N_3^+

A. Friedmann, A. M. Soliva, S. A. Nizkorodov, E. J. Bieske,* and J. P. Maier

Institut für Physikalische Chemie der Universität Basel, Klingelbergstrasse 80, 4056 Basel, Switzerland

Discrete absorptions of the N_3^+ cation assigned to the A $^3\Pi_u$ ← X $^3\Sigma_g^-$ transition have been observed between 245 and 283 nm by detecting N^+ photofragments. Rotational analysis of the (100) ← (000) band yields the following molecular constants: A $^3\Pi_{u,100}$, $T_{100-000}$ = 36 671.8 cm⁻¹, A_{100} = −39.67 cm⁻¹, B_{100} = 0.4294 cm⁻¹, r_{100} = 1.1857 Å; X $^3\Sigma_g^-$, B_0 = 0.4242 cm⁻¹, r_0 = 1.193 Å, λ_0 = 0.9125 cm⁻¹. A 2:1 alternation of rotational line intensities confirms that the ground state is centrosymmetric. As the origin of the A $^3\Pi_u$ ← X $^3\Sigma_g^-$ transition appears to be absent from the spectrum, only estimations of the A state vibrational frequencies are obtained: ν_1' = 1300 cm⁻¹, ν_2' = 440 cm⁻¹, ν_3' = 1700 cm⁻¹. In the (100)–(000) band individual rotational lines are observed with a laser limited width of 0.08 cm⁻¹, proving that the upper-state lifetime exceeds 50 ps.

Introduction

Usually molecular ions are identified mass spectroscopically long before their structures are determined experimentally. One good example is the N_3^+ cation, which appears to have first been observed more than 60 years ago in 1933.[1] Since that time many experimental investigations have addressed its formation,[2–9] reactivity,[10,11] recombination with electrons,[12] and photodissociation at several fixed wavelengths.[13] From these studies it is clear that the ion is quite strongly bound ($D_0 \approx 3.5$ eV for dissociation into N^+ (^3P) + N_2 (X $^1\Sigma_g^+$)[7,8,14]) and is produced in nitrogen plasmas through the reaction of energized N_2^+ ions (either in vibrationally excited levels of the A state[6] or in quartet states[3,7]) with N_2 molecules. Formation in the atmosphere probably involves ternary N^+ + N_2 reactions[10] to form N_3^+ in its ground state. Thus in contrast to N_2^+, which is produced in excited electronic states and is responsible for the Meinel bands,[15] its presence in the atmosphere is unlikely to be betrayed by emission. Atmospheric formation is followed by reaction with H_2O to produce H_2NO^+[10,11] or with O_2 to form NO^+.[10]

Complementing the experimental activity have been a series of ab initio calculations focusing on the cation's structure.[16–20] Although most theoretical studies concur that the molecule is linear in its ground state, there are disagreements about whether the two N—N bond lengths are equal. The first calculations in 1971 indicated a linear asymmetric geometry for the $^3\Sigma^-$ ground state with the $D_{\infty h}$ configuration lying some 15 000 cm⁻¹ to higher energy.[16] More recent theoretical efforts have concluded with both $D_{\infty h}$[19] and $C_{\infty v}$[20] minimum energy structures.

The work described in the preceding paragraphs has not to date included spectroscopic studies of the cation, although certain structural conclusions have been prompted by a photoelectron study of the N_3 radical.[14] There, an asymmetric ground-state structure was conjectured on the basis of irregular vibrational spacings in the $^3\Sigma^-$ band along with the ab initio calculations of Archibald and Sabin.[16] Perhaps the best guide to the probable properties of N_3^+ comes from gas-phase spectroscopic studies of the isoelectronic species NCN,[21–23] CCO,[24–27] and CNN.[28] All three radicals are linear and feature characteristic $^3\Pi$ ← $^3\Sigma^-$ transitions in the visible or near UV. It is not unreasonable to expect N_3^+ to share these attributes.

Experimental Section

In the spectroscopic studies described in the present paper, N_3^+ absorptions are inferred by monitoring the production of N^+ photofragments as the laser wavelength is scanned. This combination of mass spectrometry and laser spectroscopy has the advantages of unambiguous identification of the carrier and high sensitivity, with the disadvantage that measured band intensities represent a convolution of absorption and photodissociation cross sections. The resonance-enhanced N_3^+ photodissociation experiments were carried out using a tandem quadrupole–octopole–quadrupole apparatus and tuneable dye laser system.[29,30] The N_3^+ ions are created by electron bombardment in the early stages of a pulsed supersonic expansion of neat nitrogen (99.9% purity, stagnation pressure ≈ 4 bar). Rotational temperatures of molecular ions extracted from the plasma are typically 30–40 K.[30] After ionization, the beam is skimmed and injected into the first quadrupole, where mass selection of N_3^+ (m/e = 42) occurs. Following deflection through 90° by a quadrupole bender, the ions enter the octopole region where they interact with the frequency-doubled output of a pulsed dye laser. The resulting photofragments (m/e = 14) pass into a second quadrupole mass filter and continue on to a Daly ion detector.[31] The N^+ photoyield was observed to vary linearly with laser flux between 5 and 200 μJ cm⁻²/pulse suggesting a one-photon dissociation mechanism. Metastable decay of N_3^+ into either N^+ or N_2^+ ionic fragments was negligible under usual experimental conditions.

In order to investigate whether any of the vibronic bands were due to vibrationally or electronically excited ions, a strategy of recording spectra after the ions had been contained in the ion guide for up to 30 ms was sometimes adopted. Following introduction of a pulse of ions into the guide, the electrical potentials of electrostatic lenses at the entrance and exit are raised, resulting in almost complete containment of the ions. In time, due to radiative relaxation, bands involving a vibrationally or electronically excited lower state should diminish compared to bands originating in the lowest vibronic level.

Two different pulsed laser systems were used. Low-resolution spectra were taken with a Nd:YAG pumped dye laser of 0.5-cm⁻¹ resolution (Spectron Lasers). Calibration of these spectra was achieved by simultaneously recording the optogalvanic spectrum of an Fe/Ne discharge lamp. For the high-resolution spectra, an excimer-pumped dye laser equipped with an intracavity etalon (bandwidth ≈ 0.08 cm⁻¹) was employed. In this case, wavenumbers of the peaks were determined by comparison with a simultaneously measured iodine fluorescence spectrum and monitor etalon fringes.

Results

Because of the mass spectroscopic nature of the experiment, there is no doubt that N_3^+ is the photoactive species. A low
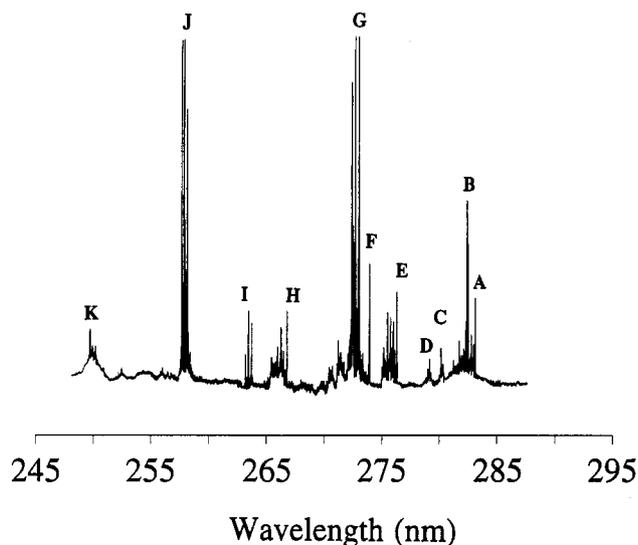
Figure 1. Low-resolution spectrum of mass-selected N_3^+ recorded by monitoring the N^+ photofragment signal in a tandem mass spectrometer system. Positions and vibronic assignments of the marked bands are listed in Table 1. The spectrum is a composite of several shorter scans made using several different laser dyes, so that relative intensities may be in error by ±50%.

TABLE 1: Wavelengths, Vacuum Wavenumbers (cm⁻¹), and Assignments for N_3^+ Bands Marked in Figure 1[a]

band	assignment	λ (nm)	energy (cm⁻¹)	displacement from origin[b]
A		283.03	35 321.4	−21.17
B		282.91	35 336.0	−6.57
C		280.01	35 702.4	359.83
D		279.02	35 829.5	486.93
E	020 ← 000	276.18	36 197.5	854.93
F		273.81	36 511.0	1168.43
G	100 ← 000	272.73	36 655.7	1313.13
H	120 ← 000	266.82	37 467.4	2124.83
I	200 ← 000	263.30	37 968.8	2626.24
J	002 ← 000	257.73	38 789.0	3446.43
K	102 ← 000	250.12	39 969.4	4626.43

[a] In bands containing more than one prominent peak, the listed value corresponds to the central component. [b] The wavenumber of the origin, which does not appear in the spectrum, has been estimated by subtracting the spacing between bands G and I from the wavenumber of band G. Unassigned bands may be due to transitions involving metastable singlet states or from vibrationally excited X $^3\Sigma_g^-$ state levels.

resolution (0.5 cm⁻¹) resonance enhanced photodissociation spectrum taken between 248 and 285 nm by monitoring the N^+ fragment intensity is reproduced in Figure 1. The spectrum is a composite recording obtained using several different laser dyes over a period of some months. Errors in the relative intensities of the different vibronic bands are estimated to be ±50%. Positions of the marked bands and their vibronic assignments (discussed below) are listed in Table 1.

Several of the vibronic bands exhibit rotational structure expected for a $^3\Pi$ ← $^3\Sigma$ transition, and the lowest energy one of these (band G) was chosen for examination under higher resolution (0.08 cm⁻¹). The resulting spectrum is shown in Figure 2, with measured line positions and assignments given in Table 2. Widths of individual lines in the high-resolution spectra appear in all cases to be laser bandwidth limited (<0.08 cm⁻¹), proving that the upper state dissociation lifetime exceeds 50 ps. It is worth emphasizing that the spectra presented in Figures 1 and 2 rely upon the detection of N^+ photoproducts and that intensities represent a convolution of absorption and dissociation cross sections and bands strong in absorption may be weak, or may not even appear in the measured spectrum. There are several examples of molecular ions (for instance CH_3I^+ [32,33]) where the
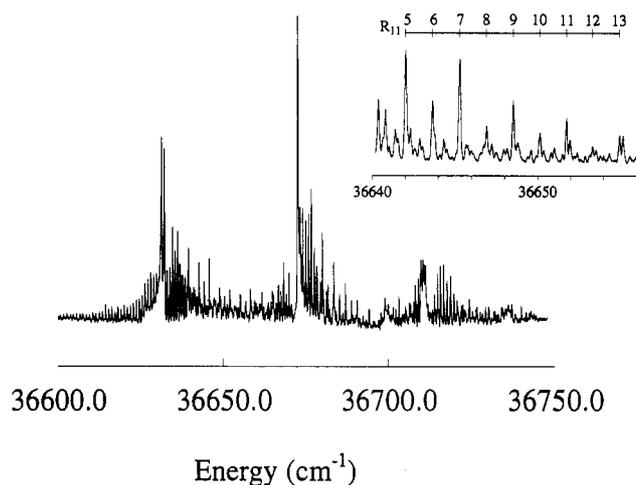
Figure 2. High-resolution (0.08 cm⁻¹) scan of the A $^3\Pi_u$ (100) ← X $^3\Sigma_g^-$ (000) band of N_3^+. The three subbands arising from transitions to the three spin–orbit components of the upper state are clearly discernible. Line wavenumbers and assignments are listed in Table 2. The inset shows a section of the R_{11} branch where the 2:1 intensity alternation of the rotational lines is clearly apparent.

origin band is absent in the resonance-enhanced photodissociation spectrum, even though transitions to higher vibronic levels appear strongly.

Vibronic Analysis

Vibronic assignments for bands displayed in Figure 1 are based on evidence from the band rotational structure, band spacings, the spectra of larger N_{2n+1}^+ complexes, and temporal variation of spectral intensities. Comparisons with the isoelectronic species NCN^{21} and CCO^{24} and ab initio calculations[16-20] lead one to expect that the lowest electronic state of N_3^+ will be of $^3\Sigma^-$ symmetry with the lowest spin allowed electronic transition to a $^3\Pi$ state. The rotational analysis shows that N_3^+ is centrosymmetric in the X $^3\Sigma_g^-$ state with only a small change in rotational constant accompanying the electronic excitation. Normally under these circumstances one would expect to see short progressions in the symmetric stretching vibration ν_1 and weak progressions involving $\Delta\nu = 0, 2, 4$ ... changes in the antisymmetric stretch vibration ν_3.

If one accepts that the origin of the A ← X transition lies at approximately 282 nm near the group of bands of lowest energy (bands A and B in Figure 1) and that the centrosymmetric structure is preserved in the A state, an obvious vibrational assignment is that band G corresponds to the (100)–(000) transition, band I to (200)–(000), band J to (002)–(000), and K to (102)–(000). The most plausible explanation for the strength of the (002)–(000) transition, which should be Franck–Condon weak, is that excitation of the antisymmetric stretch promotes coupling with the dissociative continuum. The A-state vibrational frequencies implied by this assignment are approximately $\nu_1' = 1300$ cm⁻¹, $\nu_2' = 440$ cm⁻¹, and $\nu_3' = 1700$ cm⁻¹, so that the symmetric stretch frequency is comparable to that of the isoelectronic NCN radical in its A $^3\Pi_u$ state ($\nu_1' = 1254$ cm⁻¹).[23]

The assignment discussed above implies that the origin of the A ← X transition lies at approximately 35 370 cm⁻¹ (282.5 nm), consistent with recent observations of the origin band of an N_3^+ transition in a 4 K Neon matrix at 283 nm.[34] None of the lower energy bands (A, B, or C) has the rotational structure expected for a $^3\Pi$ ← $^3\Sigma^-$ transition, and it appears probable that the origin of the A ← X transition is absent from the spectrum shown in Figure 1, due perhaps to the low photodissociation yield of the (000) level of the A state. To investigate this point further we have conducted several tests. The first of these involved trapping the ions for up to 30 ms in the octopole before irradiation. We

TABLE 2: List of Line Positions (Vacuum Wavenumbers, cm^{-1}) and Assignments for the A $^3\pi_u$ (100) ← X $^3\Sigma_g^-$ (00) Transition of N$_3$$^{+a}$

J''	$^QR_{12} + {}^OQ_{13}$	$^OP_{12}$	$^QQ_{11}$	$^PP_{11}$	$^PR_{13}$	$^PQ_{12}$	$^RR_{11}$
1		36 631.937 (01)		36 633.661 (−57)*			
2	36 628.588 (−05)	32.835 (74)*	36 632.835 (−26)*	36 635.348 (−36)*			
3	36 627.714 (20)*	36 633.588 (09)	36 633.661 (−21)*				
4	36 626.839 (17)*		36 634.487 (−11)	36 638.686 (−18)	36 623.479 (−08)		
5	36 625.953 (08)*	36 635.202 (08)	36 635.348 (40)*	36 640.364	36 621.767 (04)		
6	36 625.066 (07)*	36 636.001 (10)	36 636.111 (00)	36 642.010 (12)	36 620.016 (−15)		
7	36 624.171 (05)*	36 636.791 (10)	36 636.900 (−06)	36 643.632 (−04)*	36 618.285 (−07)		
8	36 623.273 (06)*	36 637.593 (29)	36 637.702 (07)	36 645.277 (11)*	36 616.536 (−08)	36 616.536 (−08)	
9	36 622.362 (02)*	36 638.346 (05)	36 638.455 (−23)	36 646.899 (08)	36 614.839 (49)*		
10	36 621.439 (−08)*	36 639.123 (13)	36 639.256 (03)	36 648.520 (11)	36 612.993 (−37)*		
11	36 620.528 (01)*	36 639.864 (−10)	36 640.017 (−05)	36 650.115 (−07)	36 611.256 (−07)		
12	36 619.584 (−16)*	36 640.661 (30)	36 640.797 (17)	36 651.730 (02)	36 609.475 (−16)		36 630.734 (40)
13	36 618.673 (06)*	36 641.379 (−04)	36 641.540 (−03)	36 653.333 (04)	36 607.690 (−22)	36 629.621 (10)	
14	36 617.702 (−28)*		36 642.295 (01)	36 654.949 (24)	36 605.904 (−24)		36 630.540 (18)
15	36 616.779 (−07)*	36 642.864 (−05)	36 643.037 (−02)	36 656.524 (07)	36 604.123 (−16)	36 629.402 (−15)	
16	36 615.795 (−40)*	36 643.632 (26)*	36 643.768 (−12)	36 658.103 (00)*	36 602.313 (−31)		
17	36 614.839 (−41)*	36 644.325 (−11)	36 644.523 (08)	36 659.682 (−04)	36 600.516 (−30)	36 629.196 (−09)	
18	36 613.904 (−17)*	36 645.104 (41)	36 645.277 (32)*	36 661.281 (17)	36 598.722 (−20)		
19	36 612.993 (36)*		36 645.983 (12)	36 662.848 (09)	36 596.900 (−34)	36 628.965 (−10)	
20	36 611.949 (−39)*	36 646.552 (49)	36 646.738 (45)				
21		36 647.220 (03)*		36 665.920 (−58)		36 628.831 (99)	
22		36 647.951 (23)		36 667.490 (−53)			
23				36 669.032 (−76)			
24							
25						36 628.224 (08)	
26							
27						36 627.908 (−39)	
28						36 627.714 (−98)*	

J''	$^RQ_{21}$	$^PQ_{23}$	$^QP_{21}$	$^QR_{23}$	$^SR_{21}$	$^OP_{23}$
1		36 670.805 (−12)	36 675.128 (05)*			
2	36 674.261 (−05)	36 669.999 (01)	36 676.827 (−12)	36 668.271 (−10)		
3	36 675.128 (−11)*	36 669.164 (−19)	36 678.560 (−11)	36 666.598 (−10)		36 672.627 (13)*
4	36 676.021 (−07)	36 668.366 (−10)	36 680.300 (−13)	36 664.933 (−10)		
5	36 676.902 (−17)	36 667.557 (−22)	36 682.046 (−21)		36 672.627 (00)*	
6		36 666.784 (−06)	36 683.811 (−18)	36 661.657 (17)		
7	36 678.762 (21)	36 665.999 (−13)	36 685.568 (−35)	36 660.018 (14)		
8	36 679.668 (01)	36 665.243 (00)	36 687.351 (−34)	36 658.382 (06)		36 672.921 (−41)*
9	36 680.627 (24)	36 664.475 (−09)	36 689.146 (−32)	36 656.779 (21)		
10	36 681.570 (21)		36 690.946 (−35)	36 655.163 (14)	36 672.921 (−42)*	36 673.111 (−56)*
11	36 682.517 (12)		36 692.754 (−39)	36 653.540 (−11)		36 673.227 (−57)*
12	36 683.493 (21)	36 662.337 (69)	36 694.586 (−28)	36 651.949 (−14)	36 673.111 (−55)*	36 673.413 (02)*
13	36 684.442 (−06)		36 696.406 (−41)	36 650.358 (−26)	36 673.227 (−55)*	36 673.611 (63)*
14	36 685.449 (14)	36 660.880 (38)		36 648.780 (−35)	36 673.413 (05)*	36 673.727 (32)*
15	36 686.430 (−02)	36 660.188 (44)		36 647.220 (−36)*	36 673.611 (67)*	36 673.921 (70)*
16	36 687.440 (01)	36 659.475 (18)		36 645.673 (−34)	36 673.727 (67)*	36 674.095 (77)*
17	36 688.462 (04)	36 658.783 (07)			36 673.921 (76)*	
18	36 689.510 (24)	36 658.103 (−12)*			36 674.095 (84)*	
19	36 690.476 (−49)	36 657.459 (00)				36 674.603 (28)*
20	36 691.597 (23)					36 674.860 (79)
21					36 674.603 (37)*	
22						36 675.261 (39)*
23						
24					36 675.261 (50)*	36 675.686 (−16)*
25						
26					36 675.686 (−04)*	

J''	$^QQ_{33}$	$^SR_{32}$	$^QP_{32}$	$^SQ_{31}$	$^TR_{31}$	$^RQ_{32}$	$^PP_{33}$
1			36 714.340 (36)				36 710.986 (−77)
2			36 715.254 (15)			36 710.205 (32)	
3			36 716.210 (08)				
4	36 709.494 (21)		36 717.163 (−31)				
5	36 708.794 (24)		36 718.229 (17)				
6	36 708.098 (04)	36 707.867 (05)	36 719.250 (−10)	36 719.163 (33)			
7	36 707.461 (15)	36 707.187 (02)	36 720.344 (08)	36 720.188 (12)			
8	36 706.823 (−04)	36 706.577 (41)	36 721.436 (−03)	36 721.281 (30)			
9	36 706.250 (15)	36 705.915 (00)	36 722.569 (−02)	36 722.364 (11)			
10	36 705.662 (−08)	36 705.301 (−21)	36 723.736 (07)	36 723.494 (10)			
11	36 705.109 (−23)	36 704.741 (−16)	36 724.925 (11)	36 724.663 (22)			
12	36 704.630 (08)	36 704.213 (−07)	36 726.123 (−03)	36 725.858 (32)			
13	36 704.127 (−11)		36 727.334 (−30)	36 727.035 (−01)			
14	36 703.686 (05)		36 728.593 (−35)	36 728.270 (−05)			
15	36 703.211 (−40)		36 629.891 (−28)	36 729.535 (−04)			
16	36 702.863 (18)		36 731.191 (−44)	36 730.880 (51)			
17			36 732.524 (−51)	36 732.102 (−42)			

TABLE 2 (Continued)

J''	$^QQ_{33}$	$^SR_{32}$	$^QP_{32}$	$^SQ_{31}$	$^TR_{31}$	$^RQ_{32}$	$^PP_{33}$
18			36 733.882 (−58)	36 733.461 (−23)			
19							
20					36 716.537 (13)		
21							
22					36 717.708 (27)		
23							
24							
25					36 719.568 (−35)		

a The numbers in parentheses are the difference (last two decimal places) between observed values and ones calculated using the upper and lower state Hamiltonians described in the text and the fitted constants given in Table 3. Lines marked with an asterisk are assigned more than once.

note that the intensities of several of the lower energy bands diminish with respect to others, indicating that they involve vibrationally or electronically excited N_3^+. There are predicted to be low-lying $^1\Delta$ and $^1\Sigma^+$ states[14,20] (see Figure 4), and some of the bands may involve transitions from these. In the isoelectronic NCN radical, $^1\Pi_u \leftarrow {}^1\Delta_g$ transitions have been seen in absorption in the same region as the A $^3\Pi \leftarrow$ X $^3\Sigma^-$ transition.[22]

We have also recorded spectra of N_5^+, N_7^+, and N_9^+ complexes by detecting N_3^+ photofragments. This has been done in the hope that N_2 ligands will tag the N_3^+ chromophore and will be ejected following excitation of the A $\leftarrow$ X origin transition. Binding energies for N_2 ligands in the N_3^+-$(N_2)_n$ (n = 1–6) complexes have been determined in thermochemical studies to be 4.5, 4.1, 4.1, 3.67, 3.25, and 2.44 kcal/mol,[35] much less than the 81 kcal/ mol required to break N_3^+ into N^+ + N_2. In N_3^+, coupling to the dissociative surface must occur before radiation for the transition to be mass spectroscopically detectable. However in the case of the complexes, because of the low ligand binding energies, there is also the possibility for fragmentation to occur *after* radiation to vibrationally excited levels in the ground-state manifold. This work is reported fully elsewhere,[36] and here we merely remark that for N_5^+, N_7^+, and N_9^+, although we have scanned over several thousand wavenumbers, we have observed but a single broad band (width of approximately 250 cm^{-1}), extending over the range of the A, B, C, and D bands shown in Figure 1. Given that the band lies near to the N_3^+ transitions shown in Figure 1, it seems probable that it indeed arises from a transition of an N_3^+ chromophore. Furthermore, as the band does not shift greatly with each additional N_2 ligand, one is encouraged to conclude that the origin of the N_3^+ chromophore $^3\Pi_u \leftarrow {}^3\Sigma_g^-$ transition lies nearby.

Alternative vibrational assignments to the one discussed above (for example, band G is the (001)–(000) transition, band I is (002)–(000), band J is (102)–(000), etc.) would imply that odd quanta changes in the antisymmetric stretching vibration ν_3 accompany the electronic transition, thus requiring the A state to be non-centrosymmetric, a situation difficult to reconcile with the small difference in rotational constants of upper and lower states. It is conceivable that the antisymmetric vibration becomes allowed through vibronic coupling with a nearby state of lower symmetry which is also dipole coupled to the ground state.

The (020)–(000) and (120)–(000) bands also appear to be present in the spectrum (bands E and H, respectively, in Figure 1). For the upper level, the combination of electronic and vibrational angular momentum leads to six Π and three Φ vibronic components, although only transitions to the former ones should appear strongly in the spectrum. Three effects are important in deciding the relative dispositions of the Π components: spin-orbit interactions, Renner–Teller interactions, and Fermi resonance with the higher lying (100) level. The situation has been discussed by Hougen, who gives explicit expressions for the energies.[37] Although our spectra of the (020)–(000) band exhibit heads corresponding to the expected six $\Pi \leftarrow \Sigma$ subbands, they are not of a quality sufficient for further analysis.

It is unclear whether we also observe transitions to the $^3\Pi_u$ (010) level. Because of Renner–Teller and spin–orbit interactions,

the (010) level in split into $^3\Sigma_1$, $^3\Sigma_0^{(-)}{}_+$, $^3\Delta_1$, $^3\Delta_2$, $^3\Delta_3$, $^3\Sigma_0^{(+)}{}_-$, and $^3\Sigma_1$ components with spacings determined by the Renner parameter $\epsilon\omega_2$ and the spin–orbit parameter A.[38] As the $^3\Delta_{3,2,1}$ components are expected to have the same splittings as the $^3\Pi_{2,1,0}$ components of the (000) level, the (010)–(010) band should display three subbands with the same spacings as the ones in the (100)–(000) band. Bands with this characteristic spacing are not readily discernible in the origin region of the N_3^+ spectrum. We are also unable to easily assign any of the bands immediately to higher energy from the origin, where one might expect the (010)–(000) transition. For CCO a $\Sigma \leftarrow \Sigma$ type band was observed in the corresponding region and was assigned as the A$^3\Sigma_0^{(-)}$(010) $\leftarrow$ X $^3\Sigma^-$ (000) component.

Finally we note that although we have recorded spectra of N_3^+ which are somewhat hotter than the one shown in Figure 1, we have not observed bands to the low-energy side of band A. However, the hotter spectra are distinguished by many overlapping bands lying at higher energy than the supposed origin. These are presumably due to sequences of the type (100)–(100), (001)–(001), etc., the shift to higher energy compared to the origin strongly suggesting that all three A-state vibrational frequencies are higher than the corresponding X state ones.

Rotational Analysis

Four of the vibronic bands (G, I, J, K) exhibit structure characteristic of a $^3\Pi \leftarrow {}^3\Sigma$ transition.[21,24] Of these, the one lying at lowest energy, assigned as the (100)–(000) transition (band G), was recorded under higher resolving power (0.08 cm^{-1}). This section is concerned with the rotational analysis of that band. It should be pointed out that some of our arguments parallel the ones given in the works on the NCN[21] and CCO[24] radicals. The nomenclature used to label the components of the $^3\Pi$ and $^3\Sigma$ states is standard.[21] The F''$_1$, and F''$_2$, and F''$_3$ labels in the ground electronic state correspond to components with J = N + 1, J = N, and J = $N - 1$, where J and N are quantum numbers pertaining to the total angular momentum and the angular momentum excluding spin. The F''$_2$ terms are separated from the F''$_1$ and F''$_3$ terms by the spin–spin splitting λ, which is on the order of $2B$ (see Table 3) and independent of N. The latter two terms are separated by the much smaller spin–rotation splitting, which is linearly dependent on N. For the upper $^3\Pi$ state (which is found to be inverted), the Ω = 2, 1, 0 components are labeled F'$_1$, F'$_2$, and F'$_3$, respectively.[24] An illustration of the energy levels and branches involved for a $^3\Pi \leftarrow {}^3\Sigma$ transition can be found in ref 39.

Clearly discernible in Fibure 2 are three subbands, separated by around 40 cm^{-1}, arising from transitions to the three spin-orbit components of the $^3\Pi$ state (Figure 2). Closer inspection of the spectrum reveals that the rotational constant is on the order of 0.4 cm^{-1}, so that for moderate values of J (<30) the A $^3\Pi$ state can be described by the Hund's case (a) coupling scheme. Further analysis reveals that the highest energy component shows a large λ doubling for J = 0, thus identifying it as the $^3\Pi_0$ component and proving that the A $^3\Pi_u$ state is inverted (as it is in NCN[21] and CCO[24]). The subband lying at lowest energy is

	$^3\Pi_0$	$^3\Pi_1$	$^3\Pi_2$
$^3\Pi_0$	$T^{\text{eff}} - A_v^{\text{eff}} + (B_v^{\text{eff}} - A_{Dv}) *$ $(x+1) - D_v * (x^2 + 4x + 1) + \frac{2}{3}\lambda_v$ $\pm \lambda^{\text{eff}}{}_{\perp v}$	$(2x)^{1/2} * [B_v^{\text{eff}} - 0.5 A_{Dv} - $ $2D_v * (x+1)$ $\pm 0.25 * (p_v + 2.0 * q_v)]$	$2 * (x * (x - 2))^{1/2} * (-D_v$ $\pm 0.125 * q_v)$
$^3\Pi_1$		$T^{\text{eff}} - B_v^{\text{eff}} * (x+1) - $ $D_v * (x^2 + 6x - 3) \pm 0.25 * q_v * x$ $+ \frac{4}{3}\lambda_v$	$(2 x * (x - 2))^{1/2} * [B_v^{\text{eff}} + $ $0.5 A_{Dv} - 2D_v * (x-1)]$
$^3\Pi_2$			$T^{\text{eff}} + A_v^{\text{eff}} + (B_v^{\text{eff}} + A_{Dv}) *$ $(x - 3) - D_v * (x^2 - 4x + 5) + \frac{2}{3}\lambda_v$

$$x = J * (J+1)$$

Figure 3. Hamiltonian used to model the A $^3\Pi_u$ (100) state of N_3^+. The significance of the various parameters is explained in the text. The upper and lower signs refer to the f and e levels, as defined in ref 42.

TABLE 3: Molecular Constants for N_3^+ in the X $^3\Sigma_g^-$ (000) and A $^3\pi_u$ (100) States[a]

constant	fitted values (cm^{-1})	constant	fitted values (cm^{-1})
T_v'	36 671.810(6)	p_v	
A_v'	−39.671(7)	q_v	−0.0012(1)
A_{dv}'	−0.000 10(3)	B_o''	0.424 17(9)
B_v'	0.429 43(9)	λ_o''	0.912(4)
$\lambda_{\perp v}$	1.219(8)	γ_o''	0.0003(3)

[a] Values in parentheses represent one standard deviation in the last digit. The upper and lower state centrifugal distortion constants, the upper and the lower state spin–rotation parameters, and parameter p_v were not well determined in the fit.

then identified as involving the $^3\Pi_2$ component. In this, all but one (R_{13}) of the nine expected branches could be assigned. For the central band ($^3\Pi_1 \leftarrow {}^3\Sigma_g^-$) six branches were identified and assigned. The three unobserved branches involve the F''_2 level and are predicted to have low intensities.[21] In transitions to the $^3\Pi_0$ component all but two of the branches could be at least partially assigned, the exceptions being R_{31} and P_{33}.

In all resolved branches, a clear 2:1 line intensity alternation was observed (see inset of Figure 2), evidence for the centrosymmetric structure of the lower $^3\Sigma_g^-$ electronic state. In addition, it is the odd N levels that are strong, showing that the ground state has $^3\Sigma_g^-$ or $^3\Sigma_u^+$ symmetry, the former being the only possibility consistent with the electronic configuration.[21] The central subband is almost line-like, with the other two shaded in opposite directions. This, together with the observation that only the Q-type branches show the formation of a band head, is an indication that the rotational constant changes only slightly upon excitation to the A state.

In a first analysis, some 170 lines in 10 branches were assigned. The molecular constants for the ground and the upper state of N_3^+ were obtained by a least-squares fit of the assigned line wavenumbers to a model Hamiltonian. For the $^3\Sigma_g^-$ ground state, an effective diagonal Hamiltonian can be developed:[40]

$$H_0 = B_v N^2 - D_v N^4 + {}^2/_3\lambda_v(3S_z^2 - S^2) + \gamma_v NS$$

Here, B_v is the rotational constant, D_v the centrifugal distortion

constant, λ_v the spin–spin spitting parameter, and γ_v the spin–rotation interaction parameter. In order to model the A $^3\Pi_u$ state, we have adapted the R^2 Hamiltonian shown in Figure 3, previously employed for the interpretation of the A $^3\Pi_u \leftarrow$ X $^3\Sigma^-$ transition of the isoelectronic CCO radical.[26,27,41] Included are effective terms which take into account the vibronic energy (T^{eff}), the rotational constant (B_v^{eff}), the spin–orbit splitting (A_v^{eff}), and its rotational dependence (A_{Dv}), centrifugal distortion (D_v), and λ doubling (p_v and q_v). The spin–spin interaction for two unpaired electrons is taken into account by a diagonal part (λ'), which is responsible for asymmetries in the spin–orbit splitting, and an off-diagonal contribution ($\lambda_\perp^{\text{eff}}$), which produces the λ-type splitting in the $^3\Pi_0$ $J = 0$ substate. The λ' contribution could not be fitted significantly, most probably due to its small magnitude: it is only 0.016 cm^{-1} in CCO, where the asymmetry of the spin–orbit splitting is more pronounced than in N_3^+. The upper-state spin–rotation interaction parameter γ' $^{\text{eff}}$ was constrained to 0, as it is known to be strongly correlated with the parameters for spin–orbit splitting and spin–spin interaction and cannot be fitted independently.[41] A term originally included to describe the sextic order centrifugal distortion has been omitted.

Armed with the set of molecular parameters obtained from the preliminary fit, we were able to identify many additional lines. These were usually in Q-type branches, where the lower J lines overlap to form a head, but where higher J lines are well resolved. In this way lines in 11 additional branches were assigned. The final fit was carried out with a total of 263 lines in 21 branches. The standard deviation of the fit was 0.029 cm^{-1}, comparable with the experimental resolution (0.08 cm^{-1}).

The determined molecular constants are summarized in Table 3. Note that according to the analysis, the e levels lie above the f levels for the $^3\Pi_1$ component, while for the $^3\Pi_0$ component the order is reversed. Due to the limited values of J encountered in the spectrum and our modest resolution (0.08 cm^{-1}), molecular parameters that are related to higher powers of J were not well determined. Thus, neither the upper nor lower state centrifugal distortion parameters (D'_v and D''_v) were significantly determined, and only the second of the two parameters related to the rotational dependent λ doubling in the upper state, p_v and q_v, is inferred. Similarly, the ground-state spin–rotation interaction constant was

**TABLE 4: Gas-Phase Molecular Constants (cm⁻¹) for the Isoelectronic Series N$_3$$^+$, NCN, CNN, and CCO[a]**

	N$_3$$^{+\,b}$	NCN^c	CNN^d	CCO^e
T_0	35 372	30 383.7	23 850.0	11 651.2
A_v'	−39.671	−37.56	−26.5	−35.362
A_{dv}'	−0.0001			−0.000 0269
$\lambda'_{\perp v}$	1.22	1.06		0.66
B_v'	0.4294	0.3962	0.4250	0.4066
B_v''	0.4242	0.3968	0.4136	0.3851
λ_v''	0.912	0.783	0.585	0.3864
γ_v''		−0.001		−0.000 594
ν_1'	1300	1254		2045.7
ν_1''		1232		1970.9
ν_2'	440	≈514		607.8
ν_2''		370		379.5
ν_3'	1700			1270.0
ν_3''				1063.0

^{a} Note that the A-state constants for N$_3$$^+$ are for the (100) level. Numbering of the vibrations for CCO is standard for a $C_{\infty v}$ molecule. The origin of the N$_3$$^+$ transition has been estimated by subtracting the approximate value for ν_1' from the fitted origin of the 100–000 band. ^{b} This work. ^{c} Reference 21 (with the exception of ν_1', which is from ref 23). ^{d} Reference 28. ^{e} Fine structure constants and ground-state vibrational frequencies from refs 25 and 26. The $^3\Pi$ state vibrational frequencies from ref 24.

ill defined. It should be pointed out that the (100) level will be perturbed to some extent by a Fermi resonance with the (020) level lying some 400 cm⁻¹ lower in energy. Thus, the molecular constants from the analysis should be regarded as effective parameters.

Discussion

It is interesting to compare the properties of N$_3$$^+$ determined in the present study with those of N$_3$$^-$ and N$_3$ and also with the ones of the isoelectronic radicals NCN,[21,23] CNN,[28] and CCO.[24] The molecular orbital configuration for the ground electronic state of N$_3$$^+$ is

$$1\sigma^2 2\sigma^2 3\sigma^2 4\sigma^2 5\sigma^2 6\sigma^2 1\pi^4 7\sigma^2 2\pi^2$$
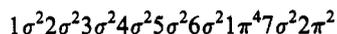
The N$_3$ and N$_3$$^-$ radicals differ by having one or two more electrons in the 2π nonbonding orbital, and consequently one would expect the vibrational frequencies and bond lengths of the three molecules to be alike. Indeed all three molecules are linear and centrosymmetric and have very similar ground-state bond lengths (N$_3$$^-$, 1.188 40 Å;[43] N$_3$, 1.181 15 Å;[44] N$_3$$^+$, 1.193 Å). The N$_3$$^+$ A-state frequencies ($\nu_1' \approx$ 1300 cm⁻¹, $\nu_2' \approx$ 440 cm⁻¹, $\nu_3' \approx$ 1700 cm⁻¹) correspond reasonably well with the N$_3$ ground-state ones ($\nu_1'' \approx$ 1320 cm⁻¹,[45] $\nu_2'' \approx$ 457 cm⁻¹,[45] $\nu_3'' \approx$ 1645 cm⁻¹ [44]), although as indicated above, the ground-state N$_3$$^+$ frequencies may be somewhat lower.

The X- and A-state properties of N$_3$$^+$ are similar in most regards to the ones of CNN, CCO, and NCN (Table 4). All four molecules have absorptions in the visible or near UV, inverted $^3\Pi$ A states, and similar vibrational frequencies and exhibit modest change in rotational constant when excited electronically. The attributes of N$_3$$^+$ are particularly close to those of NCN, both having a centrosymmetric structure and comparable A-state frequencies. For N$_3$$^+$, CNN, and CCO excitation to the A $^3\Pi_u$ upper state results in a contraction of the bond lengths, compatible in both cases with higher A than X vibrational frequencies.

Turning now to the results of previous calculations, we find that the experimental values concur best with the calculated ones in ref 19. Using a 6-311G* basis set, they predict the correct linear $D_{\infty h}$ structure, N—N bond lengths of 1.1828 Å (exptl 1.193 Å), and ground-state vibrational frequencies ν_1 = 908 cm⁻¹ and ν_3 = 1248 cm⁻¹. As mentioned above, we have not obtained ground-state frequencies but expect them to be lower than the
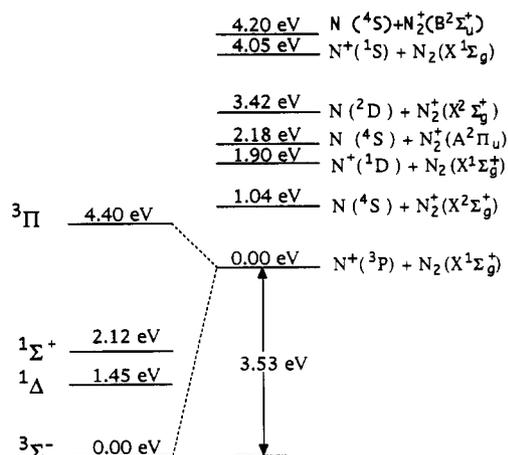

Figure 4. Low-lying bound electronic states of N$_3$$^+$ and atom plus diatomic dissociation limits. The relative spacings of the $^3\Sigma^-$ and $^1\Delta$ molecular states are taken from the ab initio calculations in ref 20, while the position of the $^1\Sigma^+$ state is from the PES studies described in ref 14. The $^3\Sigma^- - {}^3\Pi$ spacing comes from the present work. Energies for the dissociation limits are from ref 46 and 47. The 3.53-eV binding energy of the $^3\Sigma^-$ state relative to the N$^+$ (^{3}P) + N$_2$ (X $^1\Sigma_g^+$) limit is from 14. Note that the A $^3\Pi$ state of N$_3$$^+$ lies well above its adiabatic dissociation limit.

A-state ones ($\nu_1' \approx$ 1300 cm⁻¹, $\nu_2' \approx$ 440 cm⁻¹, $\nu_3' \approx$ 1700 cm⁻¹). All other calculations,[16,17,18] including the most recent (ref 20), have failed to predict the correct $D_{\infty h}$ geometry, although the latter do anticipate the spacing between the X and A electronic states reasonably well (calculated T_e = 4.93 eV, experimental T_e = 4.40 eV).

The question remains as to the mechanism responsible for the dissociation of the N$_3$$^+$ A state. The energies and relative dispositions for several of the lower lying dissociation limits of N$_3$$^+$ along with the lower bound electronic states are schematically represented in Figure 4. The limit energies are deduced from the data in ref 46 and 47, while the relative N$_3$$^+$ bound-state energies come from the ab initio calculations in ref 20, or in the case of the $^1\Sigma^+$ state from photoelectron studies of N$_3$.[14] The A $^3\Pi$–X $^3\Sigma^-$ spacing has been set to correspond to the experimentally observed transition at 282 nm. The dissociation limits and N$_3$$^+$ bound states have been offset by the experimentally determined 3.53-eV binding energy of ground-state N$_3$$^+$.[14] The dissociation limits are (energies relative to the lowest limit)

N$^+$ (^{3}P)	+	N$_2$ (X $^3\Sigma_g^+$)	(0.0 eV)
N (^{4}S^0)	+	N$_2$$^+$ (X $^2\Sigma_g^+$)	(1.04 eV)
N$^+$ (^{1}D$_2$)	+	N$_2$ (X $^1\Sigma_g^+$)	(1.90 eV)
N (^{4}S^0)	+	N$_2$$^+$ (A $^2\Pi_u$)	(2.18 eV)
N (^{2}D^0)	+	N$_2$$^+$ (X $^2\Sigma_g^+$)	(3.42 eV)
N$^+$ (^{1}S$_0$)	+	N$_2$ (X $^1\Sigma_g^+$)	(4.05 eV)
N (^{4}S^0)	+	N$_2$$^+$ (B $^2\Sigma_u^+$)	(4.20 eV)

Symmetry considerations help clarify which molecular states arise adiabatically from the various limits. For instance, as N$^+$ (^{3}P) approaches N$_2$ (X $^1\Sigma_g^+$) in a linear configuration, $^3\Sigma$ and $^3\Pi$ molecular states will be produced. These should correlate adiabatically with the X $^3\Sigma^-$ and the A $^3\Pi$ state of N$_3$$^+$. Note however that the A $^3\Pi$ state lies well *above* its adiabatic dissociation limit, despite evidence from both ab initio calculations[16–20] and our experimental results that it is at least a quasibound molecular state. Therefore, the lower $^3\Pi$ adiabatic surface must be repulsive at long range and must exhibit a barrier along the dissociation coordinate. It is possible that the barrier arises from an avoided crossing between the repulsive $^3\Pi$ surface (from the N$^+$ (^{3}P) + N$_2$ (X $^1\Sigma_g^+$) limit) and an attractive $^3\Pi$ surface from a higher limit which correlates *diabatically* with the A $^3\Pi$ state of N$_3$$^+$. Vibrational motion on the A $^3\Pi$ surface above the crossing point leads to some fraction of the molecules continuing along the repulsive surface to yield N$^+$ fragments.

Although the present work is the first to investigate a structured photoabsorption of N_3^+, there has been an earlier study of photoactivity at several fixed wavelengths.[13] Dissociation was noted at 514.5 and 488.0 nm but not at 337.1 nm. Considering the experiments described in this paper, it is almost certain that highly excited N_3^+ ions, possibly in a $^1\Sigma^+$ or $^1\Delta_g$ electronic state (see Figure 4) or with considerable vibrational energy, are responsible for these absorptions.

Conclusions

The present investigations put to an end speculations concerning the geometry of N_3^+ by showing that the ground state is linear and centrosymmetric. The small change in rotational constant on going from the X $^3\Sigma_g^-$ to the A $^3\Pi_u$ state makes it probable that the latter also has $D_{\infty h}$ symmetry. In most regards its properties are comparable to the isoelectronic species NCN, CCO, and CNN: absorption in the visible or UV, an inverted upper state with modest spin–orbit splitting (–39.7 cm^{-1}), and little geometrical change when excited to the A $^3\Pi_u$ electronic state. It is somewhat ironic that although N_3^+ was the first of these four species to be identified, it has been the last to reveal its structure.

There are several possibilities for further work. In particular, it would be desirable to observe the origin of the A $^3\Pi_u \leftarrow$ X $^3\Sigma_g^-$ transition directly, possibly by detecting the fluorescence rather than N^+ dissociation products, thereby allowing an accurate evaluation of the upper state vibrational frequencies. In addition, due to the low J values involved in the measured transitions, many of the higher order molecular constants are not well-defined by the present study. Spectra of warmer N_3^+ would help in this matter. Ab initio excited-state potential energy curves may help illuminate details of fragmentation from the A state.

References and Notes

(1) Luhr, O. *Phys. Rev.* **1933**, *38*, 459.

(2) Saporoshenko, M. *Phys. Rev.* **1958**, *3*, 1550.

(3) Cermak, V.; Hermann, Z. *Collect. Czech. Chem. Commun.* **1965**, *30*, 1343.

(4) Becker, M.; Lampe, F. W.; Cress, M. C. *J. Chem. Phys.* **1966**, *44*, 2212.

(5) Asundi, R. K.; Schulz, G. J.; Chantry, P. J. *J. Chem. Phys.* **1967**, *47*, 1584.

(6) Holland, R. F.; Maier, W. B. *J. Chem. Phys.* **1972**, *57*, 4497.

(7) Bowers, M. T.; Kemper, P. R.; Laudenslager, J. B. *J. Chem. Phys.* **1974**, *61*, 4394.

(8) Märk, T. D.; Stephan, K.; Futrell, J. H.; Helm, H. *J. Chem. Phys.* **1984**, *80*, 3185.

(9) Guthrie, J. A.; Chaney, R. C.; Cunningham, A. J. *J. Chem. Phys.* **1991**, *95*, 930.

(10) Smith, D.; Adams, N. G.; Miller, T. M. *J. Chem. Phys.* **1978**, *69*, 308.

(11) Matsuoka, S.; Nakamura, H. *J. Chem. Phys.* **1988**, *89*, 5663.

(12) Ikezoe, Y. *Chem. Phys. Lett.* **1991**, *177*, 366.

(13) Burke, R. R.; Wayne, R. P. *Int. J. Mass. Spectrom. Ion Processes* **1977**, *25*, 199.

(14) Dyke, J. M.; Jonathon, N. B. H.; Lewis, A. E.; Morris, A. *Mol. Phys.* **1982**, *47*, 1231.

(15) Meinel, A. B. *Astrophys. J.* **1950**, *112*, 562.

(16) Archibald, T. W.; Sabin, J. R. *J. Chem. Phys.* **1971**, *55*, 1821.

(17) Venanzi, T. J.; Schulman, J. M. *Mol. Phys.* **1975**, *30*, 281.

(18) Wright, J. S. *J. Am. Chem. Soc.* **1974**, *96*, 4753.

(19) Tian, R.; Facelli, J. C.; Michl, J. *J. Phys. Chem.* **1988**, *92*, 4073.

(20) Cai, Z.-L.; Wang, Y.-F.; Xiao, H.-M. *Chem. Phys.* **1992**, *164*, 377.

(21) Herzberg, G.; Travis, D. N. *Can. J. Phys.* **1964**, *42*, 1658.

(22) Kroto, H. W. *Can. J. Phys.* **1967**, *45*, 1439.

(23) Smith, G. P.; Copeland, R. A.; Crosley, D. R. *J. Chem. Phys.* **1989**, *91*, 1987.

(24) Devillers, C.; Ramsay, D. A. *Can. J. Phys.* **1971**, *49*, 2839.

(25) Yamada, C.; Kanamori, H.; Horiguchi, H.; Tsuchiya, S.; Hirota, E. *J. Chem. Phys.* **1986**, *84*, 2573.

(26) Ohashi, N.; Fujitake, M.; Kiryu, R. *J. Mol. Spectrosc.* **1992**, *154*, 169.

(27) Ohashi, N.; Kiryu, R.; Okino, S.; Fujitake, M. *J. Mol. Spectrosc.* **1993**, *157*, 50.

(28) Sarre, P. J.; Curtis, M. C.; Levick, A. P. *Laser Chem.* **1988**, *9*, 359.

(29) Bieske, E. J.; Soliva, A. M.; Maier, J. P. *J. Chem. Phys.* **1991**, *94*, 4749.

(30) Bieske, E. J.; Soliva, A. M.; Friedmann, A.; Maier, J. P. *J. Chem. Phys.* **1992**, *96*, 28.

(31) Daly, N. R. *Rev. Sci. Instrum.* **1960**, *31*, 264.

(32) McGillvery, D. C.; Morrison, J. D. *J. Chem. Phys.* **1977**, *67*, 368.

(33) Weinkauf, R.; Walter, K.; Boesl, U.; Schalg, E. W. *Chem. Phys. Lett.* **1987**, *141*, 267.

(34) Freivogel, P.; Lessen, D.; Maier, J. P. Private communication.

(35) Hiraoka, K.; Yamabe, S. *Chem. Phys. Lett.* **1989**, *154*, 139.

(36) Friedmann, A.; Nizkorodov, S.; Bieske, E. J.; Maier, J. P. *Chem. Phys. Lett.* **1994**, *224*, 16.

(37) Hougen, J. T. *J. Chem. Phys.* **1962**, *37*, 403.

(38) Hougen, J. T. *J. Chem. Phys.* **1961**, *36*, 1874.

(39) Herzberg, G. *Molecular Spectra and Molecular Structure*; Van Nostrand: Princeton, 1967; Vol. I.

(40) Hakuta, K.; Uehara, H. *J. Chem. Phys.* **1981**, *74*, 4326.

(41) Suzuki, T.; Saito, S.; Hirota, E. *J. Mol. Spectrosc.* **1985**, *113*, 399.

(42) Brown, J. M.; Hougen, J. T.; Huber, K. P.; Johns, J. W. C.; Kopp, I.; Lefebvre-Brion, H.; Merer, A. J.; Ramsay, D. A.; Rostas, J.; Zare, R. N. *J. Mol. Spectrosc.* **1975**, *55*, 500.

(43) Saykally, R. J.; Gruebele, M.; Polak, M. *J. Am. Chem. Soc.* **1987**, *109*, 2884.

(44) Brazier, C. R.; Bernath, P. F.; Burkholder, J. B.; Howard, C. J. *J. Chem. Phys.* **1988**, *89*, 1762.

(45) Beaman, R. A.; Nelson, T.; Richards, D. S.; Setser, D. W. *J. Phys. Chem.* **1987**, *91*, 6090.

(46) Moore, C. E. *Atomic Energy Levels*; National Bureau of Standards: Washington, DC, 1949; Vol. 1.

(47) Huber, K. P.; Herzberg, G. *Molecular Spectra and Molecular Structure IV. Constants of Diatomic Molecules*; van Nostrand Reinhold: New York, 1979.